


RESEARCH ARTICLE | JULY 08 2024

Simulations of nozzle gas flow and gas-puff Z-pinch implosions on the Weizmann Z-pinch

V. Tangri ; T. Queller ; E. Kroupp ; A. Dasgupta ; G. Rosenzweig ; J. L. Giuliani ; Y. Maron 



Phys. Plasmas 31, 072703 (2024)

<https://doi.org/10.1063/5.0202237>



09 July 2024 07:10:50

AIP Advances

Why Publish With Us?

-  **25 DAYS**
average time to 1st decision
-  **740+ DOWNLOADS**
average per article
-  **INCLUSIVE**
scope

[Learn More](#)



Simulations of nozzle gas flow and gas-puff Z-pinch implosions on the Weizmann Z-pinch

Cite as: Phys. Plasmas **31**, 072703 (2024); doi: 10.1063/5.0202237

Submitted: 2 February 2024 · Accepted: 15 June 2024 ·

Published Online: 8 July 2024



View Online



Export Citation



CrossMark

V. Tangri,^{1,a)} T. Queller,² E. Kroupp,² A. Dasgupta,¹ G. Rosenzweig,^{2,b)} J. L. Giuliani,³ and Y. Maron²

AFFILIATIONS

¹Plasma Physics Division, Naval Research Laboratory, Washington, DC 20375, USA

²Faculty of Physics, Weizmann Institute of Science, Rehovot 7610001, Israel

³NRL Voluntary Emeritus Program, Plasma Physics Division, Naval Research Laboratory, Washington, DC 20375, USA

^{a)}Author to whom correspondence should be addressed: varun.tangri@civ.us.navy.mil

^{b)}Present address: MKS Instruments, Wilmington, Massachusetts 01887, USA.

ABSTRACT

We present simulations of an oxygen gas puff Z-pinch on a University scale generator at the Weizmann Institute of Science. The work accounts for the detailed geometry of the nozzle, the initial neutral gas density distribution, and the subsequent implosion. The modeling results show significant improvement with data for the current at the time of stagnation in comparison with a previous effort [Rosenzweig *et al.*, Phys. Plasmas **27**, 022705 (2020)]. As a first step, we performed simulations of the flow of neutral diatomic oxygen from a plenum through a nozzle within a recessed cathode, across a gap, and into the anode with a recessed grounded honeycomb. These simulations show an agreement with the measured initial gas density profiles within the region not blocked by the recesses and accessible to visible measurements. The computed neutral gas flow profile serves as the initial condition for a radiation magnetohydrodynamic simulation of the implosion using the MACH2-TCRE code. By considering the specific details of the nozzle and chamber geometry, we find agreement with the measured current profile, including the inductive notch. The simulations predict that the plasma undergoes a strong pinch within the hidden anode recess. The simulations also predict the strongest radiation pulse occurs within the anode recess and at the time of the observed inductive notch.

© 2024 Author(s). All article content, except where otherwise noted, is licensed under a Creative Commons Attribution-NonCommercial-NoDerivs 4.0 International (CC BY-NC-ND) license (<https://creativecommons.org/licenses/by-nc-nd/4.0/>). <https://doi.org/10.1063/5.0202237>

I. INTRODUCTION

Details of the initial conditions and plasma volume play an important role in evolution of the Z-pinch gas puff implosion.¹ Some of the ways this can happen are (1) the initial density profile of the gas used at the time of initiation of discharge influences subsequent evolution, including instabilities; (2) the initial inductance and other circuit parameters influence the amount of power delivered to the plasma at any given time; and (3) the specific geometry of the chamber influences the outcome of the implosion. The effect of the initial density profile on instabilities has been investigated extensively.^{1,2} Exponential Rayleigh–Taylor (RT) growth can be suppressed as long as the implosion shock wave propagates into a load with an appropriately tailored density profile as shown theoretically,³ computationally,⁴ and experimentally.⁵ By serendipity,⁶ it was found that a double gas puff Z-pinch increased the hard x-ray (>1 keV) output by about an order of magnitude. The effect of nozzle configuration, especially the effect of having a central jet, and shell on jet has been examined extensively in a

krypton gas puff.⁷ It has been shown that the nonlinear evolution of the Z-pinch implosion dynamics also depends on the initial density distribution and mass load.^{8,9} Using simple equivalent circuits for the description of the generator and varying the circuit parameters, the effect of the generator has been discussed and investigated extensively.^{10,11} Simulations of neon on the generator at the Weizmann Institute of Science (WIS) have shown that knowledge of the initial gas density profile can be essential for matching the experimental data of the pinch.² However, the role of the load chamber geometry, particularly the electrode recesses, has not been explored to much extent. Several past and present Z-pinch facilities have recesses. One example was the University of California, Irvine (UCI) Z-pinch facility in the 90s.⁵ The TPSD shell-on-center-jet assembly on Saturn¹² had a 2 cm recess in the region between the inner and outer nozzle with a 3.8-cm A-K gap. This is almost 52% of the entire volume. Another example would be the 12-cm outer diameter triple-nozzle system¹³ designed and built by Alameda Applied Sciences Corporation (AASC) for use

on the Z generator at Sandia National Laboratories (SNL), which had a 4 cm recess with an A-K gap of only 2.5 cm. In many of the experiments with recesses, thin mesh wires positioned over the anode and cathode nozzles are often employed to establish an uninterrupted current path during the implosion process, but this approach results in the adverse consequence of causing multiple shocks within the supersonic gas flow across the imploding region, which seeds instabilities. Furthermore, it has been shown using laser induced fluorescence (LIF) measurements that the density significantly changes due to the presence of a nozzle screen.¹² Modeling the density profile due to the nozzle screen is beyond the capability of present day simulation codes used to model gas puff implosions.

Many aspects of recesses have been previously explored. In particular, the plasma density evolution within the nozzle opening during implosion for Krypton⁷ and argon gas-puffs.¹⁴ While recesses may improve certain aspects of machine efficiency, one side effect is that these may be inaccessible to diagnostics. In summary, many past and present machines have large recesses that account for a significant portion of the volume.

The present work is concerned with oxygen gas puff pinch experiments studied by Rosenzweig *et al.* on the 500 kA generator at WIS. Rosenzweig *et al.*'s first study¹⁵ describes the polarization spectroscopy of two oxygen emission lines used to diagnose the magnetic field evolution as the pinch imploded. Detailed measurements of the radial distribution of the magnetic field close to¹⁶ and in the final stage of the implosion phase¹⁷ were performed and subsequently compared with magnetohydrodynamic (MHD) simulations.^{17,18}

For these experiments, the chamber design is shown in Fig. 1. The gas nozzle is recessed axially by 5 mm from the outer edge of the cathode, the latter element forming an annular ring surrounding the exiting flow of the gas puff. The honeycomb of the anode is likewise recessed by 6 mm from an annular element with a knife edge. The knife edge on the anode structure facilitates breakdown of the oxygen gas, and the cathode recess enhances collimation of the nozzle outflow. The accessible region for all the diagnostics, including Mach-Zehnder interferometry for the initial gas density profile, was limited to the central 9 mm axial extent not blocked by the recesses.

Figure 2 displays measured current profiles from a number of oxygen puff shots on the WIS generator as thin lines. There is some variability among the current profiles, so all the currents have been

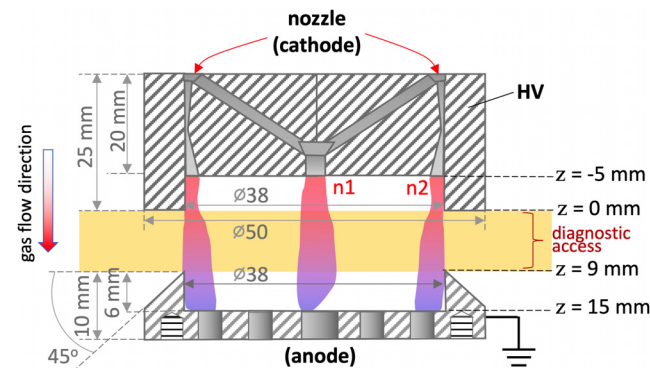


FIG. 1. Schematic diagram of the nozzle. Gas is injected from a converging-diverging cathode nozzle with a central jet (n1) and an outer shell (n2) toward the anode.

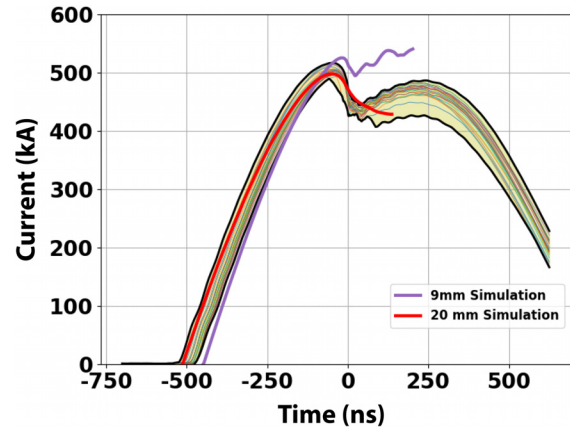


FIG. 2. Current vs time for two simulations and shots aligned by the minimum of dI/dt . The purple line indicates the simulation presented earlier, in Ref. 17 with the assumed 9 mm height. In red, a run utilizing the complete 20 mm gap data derived from a simulation of neutral gas flow is presented. The various thin lines are a set of several shots performed on the machine. The light-colored band illustrates the range of data expected due to shot-to-shot variability. This shows that among the runs presented, only the 20 mm run reproduced the notch.

aligned such that $t = 0$ refers to the minimum of dI/dt . A significant portion of this variation in implosion time arises from the shot-to-shot variation in discharge characteristics. The extent of this variability is shown as a yellow band in Fig. 2. The measured current profile yielded an implosion time of 500 ± 25 ns. In the Discussion Section of the experimental article Ref. 17, initial magnetohydrodynamic (MHD) simulations using the MACH2-TCRE code^{19,20} were presented for comparison. The initial gas density distribution for the calculations was obtained from coarse interferometry data covering the axial region from $z = 0$ to $z = 9$ mm in Fig. 1. The purple line in Fig. 2 displays the calculated current profile taken from Fig. 2 of Ref. 17. One striking feature of the simulation was the failure to reproduce the depth of the observed current notch around 0 ns in all of the measured current profiles.

The calculated current profile reaches a larger peak and does not decrease as much at the time of implosion as the data. The lack of agreement indicates inaccurate initial conditions or missing physics in the simulation. Several possible mechanisms for the discrepancy in the current profile were considered in Rosenzweig *et al.*:¹⁷ a resistive component to the load voltage in the form of a narrow current channel, anomalous resistivity, or a plasma gap with Child-Langmuir limited current. However, none of these explanations was found to be reasonable.

The inconsistency between the simulated current profile and the measured ones showing a strong inductive notch motivated us to further investigate the initial conditions of the gas puff subject to the detailed geometry of the load region. These details in the present simulations are described in Sec. II and include the recessed regions at the cathode and anode that were not accessible to the diagnostics in Ref. 17. In order to account for the initial density distribution of the oxygen puff in these “hidden” regions, it is necessary to simulate the neutral, molecular gas flow starting from the plenum and extending from the cathode to the anode electrodes. This task required enhancing the capabilities of the version of the MACH2 code used at the Naval

Research Laboratory beyond that used in Ref. 17 to include time dependent gas dynamics from a plenum through a nozzle. The results are discussed in Sec. III along with a comparison to new, absolutely calibrated, LIF data over the accessible 9 mm extent. Both LIF and interferometry have their advantages and disadvantages. LIF, which involves the use of a tracer molecule, can be used to quickly diagnose the density distribution of the gas mixture with high spatial resolution over the entire Z-pinch region, as well as its azimuthal symmetry. On the other hand, while high-sensitivity interferometry is a tracerless method that relies on fewer assumptions and is deemed more accurate, the process of obtaining chord-integrated measurements and subsequently Abel inverting them to determine local density is subject to large uncertainties near the z-axis.

In the Weizmann generator, the pulsed power is initiated while the mass flow out of the gas nozzle was still rising. If the current drive is delayed until steady state is reached, then the gas fills the region beyond the return current rods, leading to a short circuit and a poor implosion. Consequently, there is a decrease in the mass per unit axial length from the cathode nozzle to the anode. The computed neutral density profile covering the domain from the nozzle exit plane to the anode serves as the initial condition for the MHD simulations of the oxygen pinch on the WIS generator. These calculations in Sec. IV are performed with the MACH2-TCRE code that accounts for collisional-radiative equilibrium in the ionization kinetics. As expected from the axial decrease in the mass per unit length, the simulation results indicate that a zippering of the pinch occurs from the anode back toward the nozzle. Zippering is, however, less detrimental to the implosion quality than a short to the return current rods. The simulations also predict a strong pinch within the hidden anode recess coincident with the deep notch in the current profile. This notch is in good agreement with the observed current profile. Synthetic visible images are presented encompassing the diagnostically accessible region as well as the cathode and anode recesses.

Furthermore, in Sec. V, we find that the MHD simulations unexpectedly show that significantly more radiation is emitted from the anode recess than from the existing diagnostic region $0 \leq z \leq 9$ mm at early times. If diagnostic access into the recessed anode region can be engineered, then a comparison of the radiative emission from this region with that from the $0 \leq z \leq 9$ mm region would be a test of our prediction. Section VI contains a summary and conclusions.

II. LOAD GEOMETRY

The detailed load geometry is displayed in Fig. 1. The oxygen gas puff is injected as a shell on jet configuration composed of a central nozzle with an exit hole of diameter 2.6 mm, which is fed by eight circular openings each of diameter 3.6 mm. Both the central and annular nozzles are of the converging-diverging type. The cathode electrode contains the nozzle whose exit plane is recessed by 5 mm from the lower edge of an annular sleeve of thickness 6 mm. A honeycomb sits at the bottom of the anode electrode, 6 mm below the knife edge of 45° on an annular anode sleeve of 6 mm thickness. The inner diameter of both the cathode and anode recesses was 38 mm.

For the following discussion, we set the axial coordinate such that the nozzle exit plane is at $z = -5$ mm. Then the bottom of the annular cathode sleeve is at $z = 0$, the top edge of the annular anode sleeve is at $z = +9$ mm, and the honeycomb is at $z = +15$ mm. Thus, the axial extent of the region accessible to the experimental diagnostics was only 9 mm, while the total length of the pinch was 20 mm.

III. SIMULATION FOR THE INITIAL GAS PUFF DENSITY DISTRIBUTION

A precise determination of the cylindrically symmetric, two-dimensional (2D) neutral gas density distribution is needed to determine the initial conditions for the simulations of the implosion. For this, two techniques were available: The first was chordal, zero-dimensional interferometry, and the second, absolutely calibrated laser induced fluorescence (LIF). Data for both of these diagnostics were limited to $0 \leq z \leq 9$ mm. For the latter diagnostic, the emission from the gas volume, which consisted of O_2 doped with acetone vapors and excited by a laser beam, was viewed normal to the beam path with the emission focused onto a large-size CCD detector. The LIF and the chordal interferometry data were measured $(74 \pm 1) \mu s$ after the initiation of the flow of the gas from the nozzle into the ambient vacuum. The discharge is timed to about $0.5 \mu s$ after the LIF and interferometry measurement time. The $\pm 1 \mu s$ jitter is an inherent electromechanical characteristic of the pin trigger and cannot be avoided.

Since the nozzle exit plane is at $z = -5$ mm and anode honeycomb is at $z = +15$ mm, while data for the initial density distribution are restricted to $0 \leq z \leq 9$ mm, it is necessary to simulate the neutral, molecular O_2 gas flow over the entire 20 mm prior to any MHD simulation of the pinch. This is particularly the case since the generator is fired before the gas flow has reached a steady state of uniform mass per unit axial length. To simulate this initial gas distribution, we employed the MACH2 code without the ionization kinetics of the TCRE component and treat the neutral diatomic oxygen as a perfect gas with a ratio of specific heats $\gamma = 7/5$ obeying isentropic flow initial conditions. Under the assumption of cylindrical R-Z symmetry, we take advantage of MACH2's multi-block capability. The calculation domain, shown in Fig. 3, consists of 14 blocks that include the nozzle, the load region described in Sec. II, and an approximation for the plenum. The multiple block structure of MACH2 makes it possible to perform simulations of complex geometric configurations using logarithmically rectangular blocks (arrays) to describe each distinct physical region. The shape and length of the plenum is not identical to the experiment but is modeled as a long reservoir extending from $z = -25$ mm to $z = -65$ mm, of diatomic oxygen at a constant pressure of 6.9 psi, and at a density of $63 \mu g \text{ cm}^{-3}$. A long reservoir is needed to prevent unphysically large perturbations within the simulation time duration. Nevertheless, in order to compensate for the finiteness of the plenum, mass flows into the plenum at $z = -65$ mm with a density of $63 \mu g \text{ cm}^{-3}$. For numerical stability, we impose a gas background of negligible mass, lower by a factor of 10^{-3} , in the nozzle and chamber below $z = -25$ mm.

When the simulated gas valve at $z = -25$ mm opens, the gas in the plenum begins to flow into the converging-diverging annular and central nozzles at subsonic velocity. The outer edge of this annulus has a diameter of 38 mm. As the simulation progresses, the gas is injected into a chamber. Once in the chamber, the gas expands into a central jet surrounded by an annular shell at the cathode. The simulation continues as the gas exits through the anode honeycomb at the lower boundary, where the anode honeycomb lies. In the neutral gas density calculation, the skirt (which is a physical part of the nozzle) was included, but the anode knife-edge was assumed to be absent. The experimental measurements, on the other hand, were conducted utilizing the knife-edge anode. The experiments reveal that the impact of reflections from the anode structure on gas distribution becomes

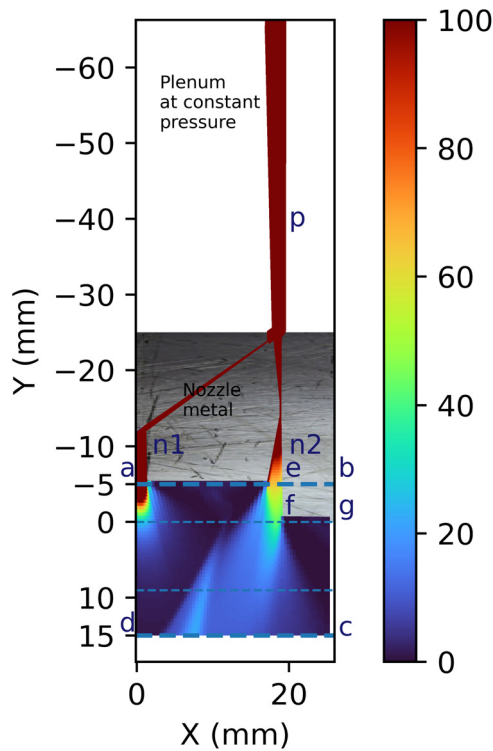


FIG. 3. A diagram of the geometry for the neutral gas simulations assuming R-Z symmetry including the plenum, nozzle, and chamber used in the simulations. A plenum at constant pressure (colored red and marked p) injects gas into a nozzle with two openings (marked n1 and n2) and a chamber with a low density (blue). The units of the color bar are g cm^{-3} .

apparent only after a time interval of $150 \mu\text{s}$. As such, a comparison between the calculations and the measurements remains reasonable. The simulation indicates that it takes $200 \mu\text{s}$ for the gas flow to reach steady state, which is much longer than the time between the opening of the gas valve and the initiation of the HV discharge.

The computed gas density profiles in $\mu\text{g cm}^{-3}$ at $z = -2.5, 2, 4, 6, 8, \text{ and } 11 \text{ mm}$ are shown in Figs. 4(a)–4(f) as solid black lines. These results are compared with the measured absolutely calibrated LIF densities at $(74 \pm 1) \mu\text{s}$ shown as red lines in Figs. 4(b)–4(e). The blue bands indicate uncertainty in measurement data. We find that within the diagnostically accessible region, there is a fairly good agreement between the neutral flow simulation and the measurements.

Clearly, the peak density decreases as z increases. Figure 5 shows the linear mass density, $\int \rho(r, z) 2\pi r dr$ in $\mu\text{g/cm}$, along the axial coordinate from the nozzle exit plane to the anode honeycomb. The diagnostically accessible region ($0 \leq z \leq 9 \text{ mm}$) is marked by vertical dashed lines and contains the linear mass density from the LIF measurements. In this region, there is a good agreement between the neutral flow calculation and the data, thereby supporting the accuracy of the modeling, as indicated in Fig. 4. The significant point is the strong decrease in linear mass density across the extent from the cathode recess, through the visible region, and into the anode recess. This decrease is important for the MHD simulations of the pinch.

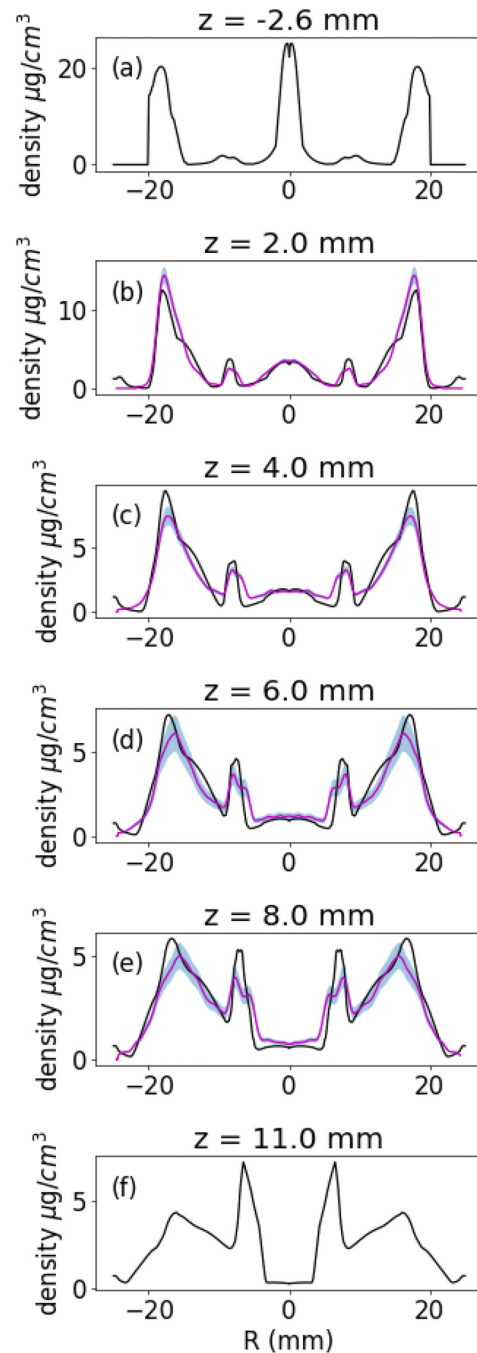


FIG. 4. Variation of density in $\mu\text{g cm}^{-3}$ for various axial positions is shown in (a)–(f). (b)–(e) The absolutely calibrated LIF measurement data in red in the observable window. Also shown in (b)–(e) are the error estimates in blue. The computational results are shown in black, including predictions in the cathode recess (a) as well as the anode recess (f).

A number of simulations investigating the effect of parameters such as viscosity, plenum pressure, and measurement jitter were also made. The doubling of the plenum pressure from 10 to 20 psi resulted in a substantial increase in the mass within the chamber, growing from

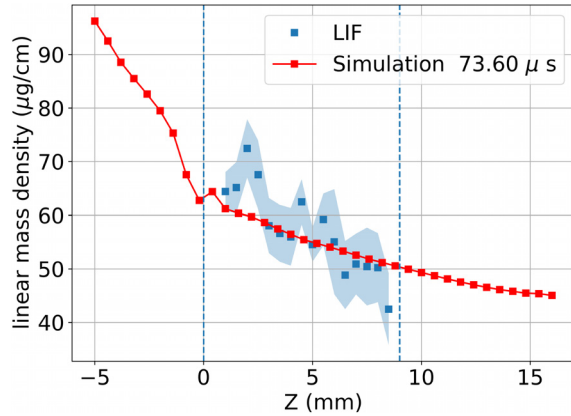


FIG. 5. The absolutely calibrated LIF data (blue squares) with error bands (light blue). Also shown here is the MHD simulation initial data (solid red line). The diagnostically accessible region in which measurements can be made is indicated by the vertical dashed lines.

98.6 to 189.2 μg . Although this represents a near doubling of the original mass, there was only a 4% decrease from the expected increase. This deviation may be due to the numerical approximations, model simplifications, and nonlinearities present in fluid dynamics.

Within the parameter regime of the simulations, the impact of viscosity on the results was also examined and was determined to have a minimal effect. Despite its significance in fluid dynamics, the contribution of viscosity in this particular scenario was found to be limited in comparison to other factors.

Finally, the role of the 1 μs jitter was also examined using data at several time steps. Data were analyzed at 73.4 and 74.4 μs to determine the effect of this deviation. The results showed that a 1 μs jitter in measurement caused a negligible change of 0.2% in the total mass. This finding highlights the robustness of the measurement process, as well as the accuracy of the simulation data.

IV. MHD SIMULATION OF THE PINCH

With the initial gas density computed in Sec. III, we can now model the magneto-hydrodynamics of the oxygen pinch on the WIS generator, including the recessed regions in the cathode and anode. This simulation is done with MACH2-TCRE, an Arbitrary Lagrangian-Eulerian (ALE) resistive MHD simulation code.²⁰ The MHD algorithm calculates three components of the velocity and of the magnetic field along with the mass density in a 2D, R-Z geometry assuming azimuthal cylindrical symmetry. In order to account for the non-LTE ionization dynamics, including opacity and non-local transport, the tabular collisional-radiative equilibrium (TCRE) database model of radiation transport has been employed along with a self-consistent equation of state for oxygen. In the TCRE model, a table lookup is performed using a table entry that is characterized by three parameters: (1) specific internal energy that includes electron thermal as well as excitation/ionization, (2) ion density, and (3) opacity. Using this table, the MHD solution including radiation transport, average charge, and electron temperature can be computed. Details of the TCRE method are explained by Thornhill *et al.*^{19,20} This method is very efficient and enables multi-dimensional R-Z simulations with collisional-radiative conditions for the ionization kinetics. Given that

there is a pre-ionizer in the WIS experiment, we initialize the MHD simulation by assuming the molecular gas in the neutral gas flow calculation is now fully dissociated and uniformly ionized with two free electrons per ion with a uniform electron temperature of 3 eV.

In our calculations, the generator will be treated as a lumped circuit, but the load region will be modeled in more detail. The circuit consists of a capacitor bank (5.5 μF), charged to 60 kV, in series with a resistor (20 m Ω), and an inductor (30 nH). Into a dead short load, the generator delivers a peak current of 500 kA, rising in 500 ns, as measured by a calibrated B-dot probe. A pre-ionizer of high energy electrons was used in order to improve the reproducibility of the of the oxygen gas puff.

Simulations used the characteristics of the lumped model described above and is self-consistently coupled with the magneto-hydrodynamics in MACH2-TCRE in order to simulate the Z-pinch dynamics. The initial radius of the simulation was 25 mm. The plasma return current radius was 67.5 mm, which corresponds to an initial inductance of 4 nH using 20 mm for the axial length. The calculation domain covers the region “abcd” of Fig. 3, i.e., the outer radius of 25 mm includes the annular sleeves of the cathode and anode electrodes that were modeled using a low density plasma. Low density plasma was used because the TCRE component of the code involves rays that traverse the entire plasma to handle the radiation transport, i.e., it is not just a local transport out of an emitting cell but accounts for possible absorption in distant cells. However, at this time, the TCRE component is limited to a rectilinear cylinder and cannot handle the electrode sleeves.

At stagnation, a hot and dense core forms on axis, typically for 10 ns. The characteristic values at stagnation of the electron density $n_e \sim 10^{20} \text{cm}^{-3}$ and electron temperature, $T_e \sim 200 \text{eV}$, were previously determined for a neon puff under similar conditions.^{21–23} The red curve in Fig. 2 shows the computed current profile when the entire cathode–anode gap of 20 mm is included in the MHD simulation. We see that the modeled current profile now captures the strong notch displayed by the experimental profiles, while the purple current profile in Fig. 2 from the simulation in Ref. 17 does not capture the notch. This is because it only modeled the pinch in the diagnostically available region between $z = 0$ and 9 mm. We note that the computations were halted at 125 ns and that the red curve does not follow the subsequent rise in the data following the notch. The observed feature indicates a reduction of the load inductance due to a re-expansion of the current channel or the onset of a current shunt prior to the plasma load. Further research is planned to investigate this issue.

This simulated stagnation is seen in Fig. 6, which displays the 2D color plot of the evolution of the plasma mass density in $\mu\text{g cm}^{-3}$ of the oxygen pinch at five different times: (a) -100ns , (b) -50ns , (c) -20ns , (d) -10ns , and (e) 1 ns. As in Fig. 2, the fiducial zero time is that of minimum dI/dt . Note that the minimum and maximum density is different for each sub-figure in order to improve the contrast. The horizontal dashed lines indicate the diagnostically accessible region ($0 \leq z \leq 9 \text{mm}$) in which measurements can be made. At $t = -100 \text{ns}$, the peak density is low, $\sim 40 \mu\text{g cm}^{-3}$; however, it rises by a factor of 75 in roughly 100 ns. The peak mass density at $t = 1 \text{ns}$ is $\sim 3.5 \times 10^3 \mu\text{g cm}^{-3}$, which is an ion density of approximately 10^{20}cm^{-3} and is located in the anode recess ($9 \leq z \leq 15 \text{mm}$). The corresponding electron density is $\sim 7 \times 10^{20} \text{cm}^{-3}$. One sees in the bottom-two sub-figures that the plasma implodes first in the anode

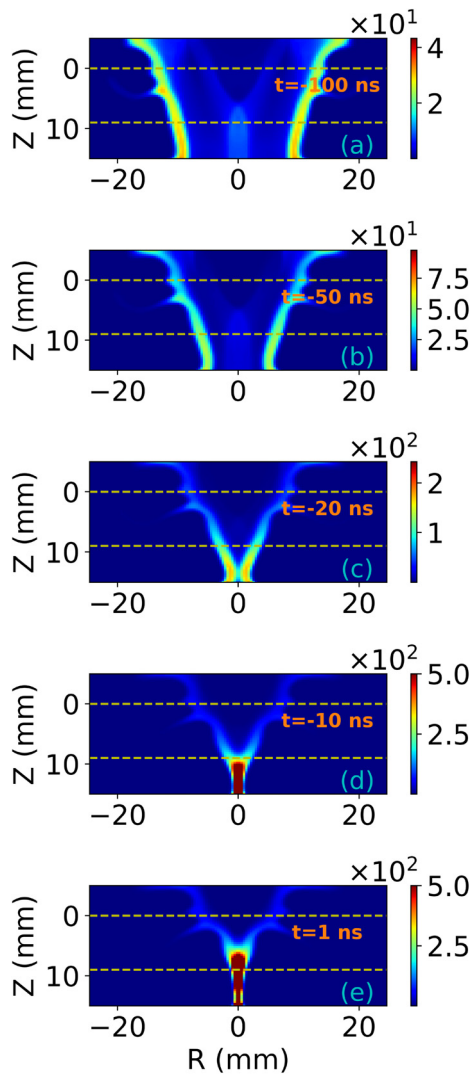


FIG. 6. Plasma density colormap at various times. The units of the mass density are $\mu\text{g cm}^{-3}$ as in Fig. 4. The diagnostically accessible region ($0 \leq z \leq 9$ mm) in which measurements were made is indicated by the horizontal dashed lines.

recess in a tight pinch at $z \sim 12$ mm and is densest there, while the plasma in the region $0 \leq z \leq 9$ mm is still relatively far from the axis.

The agreement with the measured current profile in the present work arises because there is a tight stagnation of the gas puff within the anode recess. The tight pinch within the anode recess produces a large inductance change that causes the deep current notch, since the inductance is a function of the plasma radius. Figure 7 shows the temporal evolution of the plasma radius at five different axial locations: $z = -4, 2, 4, 8,$ and 12 mm during the implosion. The mass weighted plasma radius ($r = \sum r_{ij}m_{ij}/M$, where i, j refer to zone indices and M is the total mass) is used as a metric for the plasma radius. The location $z = -4$ mm is in the cathode recess and $z = 12$ mm is in the anode recess, while the remaining three values of z are in the diagnostically accessible region. Because of the low mass in the anode recess at the

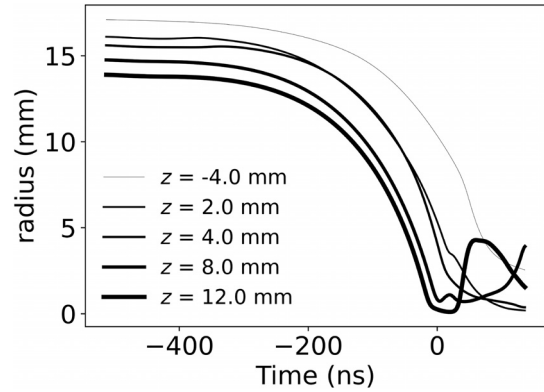


FIG. 7. Plasma radius vs time for various values of z .

time of initiation of the discharge, the plasma here gains kinetic energy earlier and also stagnates earlier. Thus, another consequence of Figs. 6(a)–6(e) and 7 is that the implosion velocity depends on the value of z .

The implosion clearly exhibits a zippering that proceeds from the anode recess back toward the cathode in time. This zippering results from the strong gradient in the initial linear mass density shown in Fig. 5. Zippering can produce a much longer radiation pulse than expected from a 1D implosion.

The change in inductance was compared for the simulated pinch between 0 and 9 mm and the one covering the full extent of the load by analyzing the ratio $2E_b/I^2$, where E_b represents the magnetic energy. As the plasma undergoes compression, this ratio exhibits a continuous and monotonic increase, reaching 4.9 nH for the 9 mm simulation and 9.7 nH for the 20 mm simulation. A significant factor contributing to this increase is the extended length of the plasma.

V. RADIATIVE PREDICTIONS

Our calculations indicate that the inductive notch in the observed current profile arises because the plasma undergoes a tight pinch within the hidden recess at the downstream anode. In this section, we predict two radiative properties of the pinch that could be used to test our conjecture if diagnostic access through the anode skirt could be manufactured. Figure 8 shows the total radiative power emitted from two parts of the plasma: the entire 9–15 mm anode recess (dashed line) and the 4–6 mm narrow slit (solid line) that is accessible to current diagnostics such as a photo conductive detector (PCD). Since the pinch first gets denser and hotter in the anode recess, the radiation from this volume precedes the peak from the 4–6 mm observable window. In our simulations, this delay was about ~ 17 ns. The radiation from the 4–6 mm narrow slit was nearly symmetric with a peak of 5.9 GW (i.e., 2.95 GW mm^{-1}) and a full width at half maximum of ~ 13.3 ns. The peak radiation from the entire anode recess was observed at $t = -4.2$ ns to be about 19.8 GW (i.e., 3.05 GW mm^{-1}) with a pulse of approximate width of ~ 20 ns. However, at this particular time, the radiation from the narrow 4–6 mm slit is only 0.15 GW mm^{-1} . Not shown in the figure is the entire radiation pulse including all the diagnostically inaccessible regions. This pulse was wider than either of the above-mentioned pulses and had multiple peaks and a peak power of about 23.8 GW. Note that not all of the radiation from the slit would be detected by a PCD. One source of

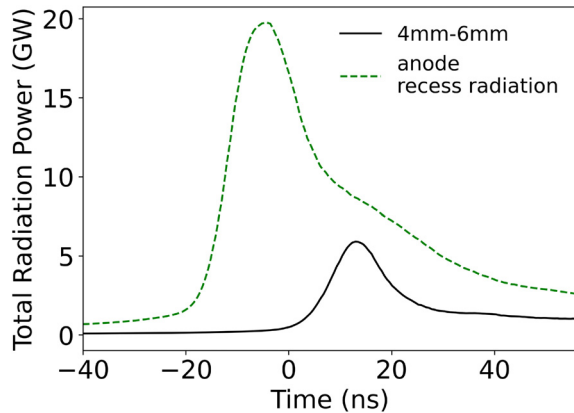


FIG. 8. The radiation emitted from two different parts of the plasma is shown: the 4–6 mm plasma window (solid line) and the anode r recess (dashed line). Notably, the radiation pulse from the recess reaches its peak earlier than the pulse from the 4 to 6 mm window. The $t = 0$ on the x-axis corresponds to the minimum point of dI/dt .

possible variation is that the 4–6 mm slit is narrow and may lead to different results on each shot. However, it is expected that the presence of a tight pinch that is bright in the anode recess would be a constant feature. These characteristics would not have been detectable using the existing diagnostics.

Figure 9 presents a synthetic image of the computed emission of the implosion at the time of stagnation within the anode recess. This corresponds in time to Fig. 6(c), which is well before the minimum dI/dt but is closest to the time when the pinch begins to form. The computation assumes only Bremsstrahlung radiation in the visible region at a wavelength of $\lambda = 380$ nm. To compute the image, plasma properties were converted from cylindrical r - z coordinates to Cartesian x - y - z coordinates and many parallel rays, denoted by their location x - y , were cast normal to the pinch axis. The radiative transport equation for absorption (α_ω) and emissivity (j_ω)

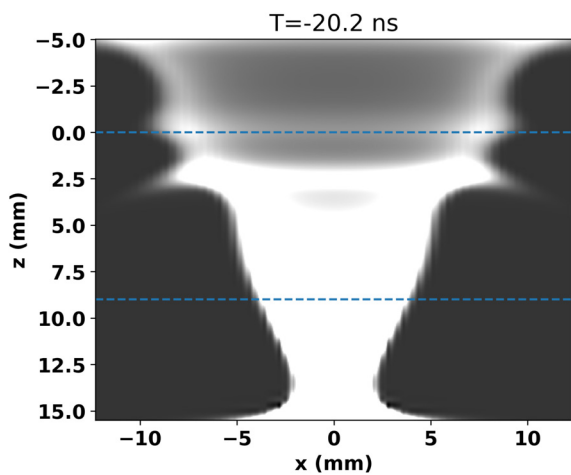


FIG. 9. Synthetic visible image of the plasma created at a single wavelength of 380 nm.

$$I_\omega(x, y) = \int_0^{s(x,y)} j_\omega(s') e^{-\int_{s'}^{s(x,y)} \alpha_\omega(s'') ds''} ds' \quad (1)$$

was solved along each ray, with s denoting the path length. The lower limit of the integral is at the far end of each ray, intersecting the plasma cylinder and we assume no incident radiation at this point. The transport coefficients were taken from Ref. 24.

Both the total radiative power and the synthetic image could be compared to experimental imaging if access to the anode recess could be provided by an observation slit through the anode annular sleeve. This is the brightest part of the pinch; hence, a significant portion of the radiation is not captured by existing diagnostics.

VI. SUMMARY AND CONCLUSIONS

In this paper, it was argued that the specific geometry of the chamber influences the outcome of the implosion. To this end, the role of modeling the diagnostically inaccessible recesses that have direct bearing on the plasma dynamics in the implosion chamber was investigated. It was shown that modeling these recesses is important while simulating the evolution of the implosion. However, modeling of MHD implosions cannot be done reliably if initial density profile in the recesses is not available. Accurate knowledge of the initial density is important because it is well known that the initial density profile of the gas used at the beginning of the implosion phase, influences subsequent evolution including instabilities. An experiment at WIS¹⁷ was examined where the initial density data from an absolutely calibrated LIF, interferometry, as well as the subsequent spectroscopic measurements of the implosions were limited to a 9 mm axial extent. While modeling these implosions in Ref. 17 using the MHD code MACH2-TCRE, a conundrum arose, namely, that the simulations failed to reproduce the depth of the observed current notch. A number of conjectures as to what could be responsible for the observed deep current notch were examined, and none of these explanations was found to be reasonable.

While examining the experimental chamber design, it was realized that two recesses of height 5 and 6 mm in the chamber should have a bearing on the MHD dynamics. Without knowledge of initial density at those locations, it was necessary to simulate the entire flow of neutral diatomic oxygen from the plenum through the nozzle and into the load chamber. Data from simulations taken at $73.6 \mu\text{s}$ were compared with the absolutely calibrated LIF measurements in Fig. 4. We found that within the diagnostically accessible region, there is a fairly good agreement between the neutral-gas flow simulation and the measurements. It was shown in Fig. 5 that there is a strong decrease in linear mass density across the extent from the cathode recess, through the visible-gap region, and into the anode recess. The reason for the strong decrease is that the neutral gas-flow at $73.6 \mu\text{s}$ has not yet reached steady state. This decrease in mass density along z naturally led to zippering in the MHD simulations of the pinch. A number of simulations investigating the effect of parameters were also made. Simulations also showed that a $1 \mu\text{s}$ jitter in the time of measurement caused a negligible change of 0.2% in the total mass.

Using the density profile computed from the aforementioned neutral gas simulations, it was possible to model the magnetohydrodynamics of the oxygen pinch using MACH2-TCRE. The red curve in Fig. 2 shows the computed current profile when the entire cathode–anode gap of 20 mm is included in the MHD simulation. We see that the modeled current profile now captures the strong notch displayed

by the experimental profiles, while the purple current profile in Fig. 2 from the simulation done in Ref. 17 does not capture the notch, because it only modeled the pinch in the diagnostically available region between $z = 0$ and 9 mm. The agreement in the present work arises because there is a tight stagnation of the gas puff within the anode recess and a consequent large increase in the load inductance. Figure 6 displays the 2D plot of the evolution of the mass density at five different time points. The plasma implodes first in the anode recess in a tight pinch and is densest there, while the plasma in the region $0 \leq z \leq 9$ mm accessible to diagnostics is still far from the axis. The presence of a tight pinch in the anode recess would not have been detectable using currently installed diagnostics. Figure 7 shows the temporal evolution of the plasma radius at five different axial locations during the implosion. The evolution exhibits a zippering that proceeds from the anode recess back toward the cathode in time. This zippering results from the strong gradient in the initial linear mass density shown in Fig. 5. The percentage of radiation emitted from the recesses was found to be significant as shown in Fig. 8. Since the pinch first gets denser and hotter in the anode recess, the radiation from this area precedes the peak from the 4–6 mm by about ~ 17 ns. The radiation from the narrow slit was nearly symmetric, with a peak of 5.9 GW and a full width at half maximum of ~ 13.3 ns.

Using Bremsstrahlung radiation from at 380 nm, Fig. 9 presents a synthetic image of the implosion at a time when stagnation has happened in the anode recess but not in the diagnostically accessible region. If a slit hole were drilled through the anode annular sleeve for observations, then the synthetic image could be compared to experimental imaging. This is the brightest part of the pinch; hence, a significant portion of the radiation is not captured by the current diagnostics. In conclusion, recesses can play an important role in regulating the dynamics of Z-pinch. This study can help us understand the dynamics of many other devices that have recesses and have not been explored extensively. In order to fully understand the notch, we have to know the true inductance and, therefore, we need to compare the measured magnetic field with the simulations. Corresponding experimental work is currently being performed at the WIS and will be discussed in a future publication. In this paper, we have not discussed the effect of the recesses on the magnetic field profile and the role of the obstructions shape on MHD dynamics. They will be the focus of future work.

ACKNOWLEDGMENTS

The authors would like to gratefully acknowledge frequent discussions with Sasha Velikovich at NRL. This work is supported by the DOE/NNSA through Interagency Agreement (IAA) No. 89233121SNA000268. The Weizmann authors acknowledge the invaluable discussions with Amnon Fisher. This work was supported in part by the DOE/National Nuclear Security Administration (NNSA) via the U.S. Naval Research Laboratory, in part by the USA-Israel Binational Science Foundation and in part by the Cornell Multi-University Center of Excellence for High Energy Density Science (USA).

Distribution statement A: Approved for public release, distribution is unlimited.

AUTHOR DECLARATIONS

Conflict of Interest

The authors have no conflicts to disclose.

Author Contributions

V. Tangri: Conceptualization (lead); Formal analysis (lead); Investigation (lead); Methodology (lead); Validation (lead); Visualization (lead); Writing – original draft (lead); Writing – review & editing (lead). **T. Queller:** Data curation (equal); Writing – review & editing (equal). **E. Kroupp:** Writing – review & editing (supporting). **A. Dasgupta:** Funding acquisition (lead); Resources (equal). **G. Rosenzweig:** Data curation (supporting). **J. L. Giuliani:** Supervision (equal); Writing – review & editing (equal). **Y. Maron:** Funding acquisition (supporting); Resources (equal); Supervision (equal).

DATA AVAILABILITY

The data that support the findings of this study are available from the corresponding author upon reasonable request.

REFERENCES

- J. L. Giuliani and R. J. Comisso, "A review of the gas-puff Z-pinch as an x-ray and neutron source," *IEEE Trans. Plasma Sci.* **43**, 2385–2453 (2015).
- J. L. Giuliani, J. W. Thornhill, E. Kroupp, D. Osin, Y. Maron, A. Dasgupta, J. P. Apruzese, A. L. Velikovich, Y. K. Chong, A. Starobinets, V. Fisher, Y. Zarnitsky, V. Bernshtam, A. Fisher, T. A. Mehlhorn, and C. Deeney, "Effective versus ion thermal temperatures in the Weizmann Ne Z-pinch: Modeling and stagnation physics," *Phys. Plasmas* **21**, 031209 (2014).
- A. L. Velikovich, F. L. Cochran, and J. Davis, "Suppression of Rayleigh-Taylor instability in Z-pinch loads with tailored density profiles," *Phys. Rev. Lett.* **77**, 853–856 (1996).
- J. H. Hammer, J. L. Eddleman, P. T. Springer, M. Tabak, A. Toor, K. L. Wong, G. B. Zimmerman, C. Deeney, R. Humphreys, T. J. Nash, T. W. L. Sanford, R. B. Spielman, and J. S. De Groot, "Two-dimensional radiation-magnetohydrodynamic simulations of Saturn imploding Z pinches," *Phys. Plasmas* **3**, 2063–2069 (1996).
- A. G. Roussikh, A. S. Zhigalin, V. I. Oreshkin, N. A. Labetskaya, S. A. Chaikovskiy, A. V. Batrakov, G. Y. Yushkov, and R. B. Baksht, "Study of the stability of Z-pinch implosions with different initial density profiles," *Phys. Plasmas* **21**, 052701 (2014).
- T. Chang, A. Fisher, and A. Van Drie, "X-ray results from a modified nozzle and double gas puff Z pinch," *J. Appl. Phys.* **69**, 3447–3450 (1991).
- C. A. Jennings, D. J. Ampleford, D. C. Lamppa, S. B. Hansen, B. Jones, A. J. Harvey-Thompson, M. Jobe, T. Strizic, J. Reneker, G. A. Rochau, and M. E. Cuneo, "Computational modeling of krypton gas puffs with tailored mass density profiles on Z," *Phys. Plasmas* **22**, 056316 (2015).
- M. A. Liberman, J. S. De Groot, T. A., and R. B. Spielman, *Physics of High-Density Z-Pinch Plasmas* (Springer-Verlag, New York, 1999).
- M. R. Douglas, J. S. de Groot, and R. B. Spielman, "The magneto-Rayleigh-Taylor instability in dynamic z pinches," *Laser Part. Beams* **19**, 527–540 (2001).
- J. W. Thornhill, Y. K. Chong, J. P. Apruzese, J. Davis, R. W. Clark, J. L. Giuliani, R. E. Terry, A. L. Velikovich, R. J. Comisso, K. G. Whitney, M. H. Frese, S. D. Frese, J. S. Levine, N. Qi, H. Sze, B. H. Failor, J. W. Banister, P. L. Coleman, C. A. Coverdale, B. Jones, and C. Deeney, "One- and two-dimensional modeling of argon k-shell emission from gas-puff Z-pinch plasmas," *Phys. Plasmas* **14**, 063301 (2007).
- J. W. Thornhill, J. L. Giuliani, Y. K. Chong, A. L. Velikovich, A. Dasgupta, J. P. Apruzese, B. Jones, D. J. Ampleford, C. A. Coverdale, C. A. Jennings, E. M. Waisman, D. C. Lamppa, J. L. McKenney, M. E. Cuneo, M. Krishnan, P. L. Coleman, R. E. Madden, and K. W. Elliott, "Two-dimensional radiation MHD modeling assessment of designs for argon gas puff distributions for future experiments on the refurbished Z machine," *High Energy Density Phys.* **8**, 197–208 (2012).
- S. L. Jackson, B. V. Weber, D. Mosher, D. G. Phipps, S. J. Stephanakis, R. J. Comisso, N. Qi, B. H. Failor, and P. L. Coleman, "A comparison of planar, laser-induced fluorescence, and high-sensitivity interferometry techniques for gas-puff nozzle density measurements," *Rev. Sci. Instrum.* **79**, 10E717 (2008).

- ¹³M. Krishnan, K. W. Elliott, R. E. Madden, P. L. Coleman, J. R. Thompson, A. Bixler, D. C. Lamppa, J. L. McKenney, T. Strizic, D. Johnson, O. Johns, M. P. Vigil, B. Jones, D. J. Ampleford, M. E. Savage, M. E. Cuneo, and M. C. Jones, "Architecture, implementation, and testing of a multiple-shell gas injection system for high current implosions on the Z accelerator," *Rev. Sci. Instrum.* **84**, 063504 (2013).
- ¹⁴A. J. Harvey-Thompson, C. A. Jennings, B. Jones, J. P. Apruzese, D. J. Ampleford, D. C. Lamppa, C. A. Coverdale, M. E. Cuneo, J. L. Giuliani, S. B. Hansen, M. C. Jones, N. W. Moore, G. A. Rochau, and J. W. Thornhill, "Investigating the effect of adding an on-axis jet to Ar gas puff Z pinches on Z," *Phys. Plasmas* **23**, 101203 (2016).
- ¹⁵G. Rosenzweig, E. Kroupp, A. Fisher, and Y. Maron, "Measurements of the spatial magnetic field distribution in a Z-pinch plasma throughout the stagnation process," *J. Instrum.* **12**, P09004 (2017).
- ¹⁶G. Davara, L. Gregorian, E. Kroupp, and Y. Maron, "Spectroscopic determination of the magnetic-field distribution in an imploding plasma," *Phys. Plasmas* **5**, 1068–1075 (1998).
- ¹⁷G. Rosenzweig, E. Kroupp, T. Queller, A. Starobinets, Y. Maron, V. Tangri, J. L. Giuliani, and A. Fruchtman, "Local measurements of the spatial magnetic field distribution in a Z-pinch plasma during and near stagnation using polarization spectroscopy," *Phys. Plasmas* **27**, 022705 (2020).
- ¹⁸V. Tangri, J. L. Giuliani, A. Dasgupta, T. Queller, E. Kroupp, and Y. Maron, "Recent simulations of nozzle gas flow and gas-puff Z-pinch implosions with magnetic fields in the Weizmann Z-pinch," in *2021 IEEE International Conference on Plasma Science (ICOPS)* (IEEE, 2021).
- ¹⁹J. W. Thornhill, J. P. Apruzese, J. Davis, R. W. Clark, A. L. Velikovich, J. L. Giuliani, Y. K. Chong, K. G. Whitney, C. Deeney, C. A. Coverdale, and F. L. Cochran, "An efficient tabulated collisional radiative equilibrium radiation transport model suitable for multidimensional hydrodynamics calculations," *Phys. Plasmas* **8**, 3480–3489 (2001).
- ²⁰J. W. Thornhill, J. L. Giuliani, B. Jones, J. P. Apruzese, A. Dasgupta, Y. K. Chong, A. J. Harvey-Thompson, D. J. Ampleford, S. B. Hansen, C. A. Coverdale, C. A. Jennings, G. A. Rochau, M. E. Cuneo, D. C. Lamppa, D. Johnson, M. C. Jones, N. W. Moore, E. M. Waisman, M. Krishnan, and P. L. Coleman, "2-D RMHD modeling assessment of current flow, plasma conditions, and Doppler effects in recent z argon experiments," *IEEE Trans. Plasma Sci.* **43**, 2480–2491 (2015).
- ²¹E. Kroupp, D. Osin, A. Starobinets, V. Fisher, V. Bernshtam, Y. Maron, I. Uschmann, E. Förster, A. Fisher, and C. Deeney, "Ion-kinetic-energy measurements and energy balance in a Z-pinch plasma at stagnation," *Phys. Rev. Lett.* **98**, 115001 (2007).
- ²²E. Kroupp, D. Osin, A. Starobinets, V. Fisher, V. Bernshtam, L. Weingarten, Y. Maron, I. Uschmann, E. Förster, A. Fisher, M. E. Cuneo, C. Deeney, and J. L. Giuliani, "Ion temperature and hydrodynamic-energy measurements in a Z-pinch plasma at stagnation," *Phys. Rev. Lett.* **107**, 105001 (2011).
- ²³D. Alumot, E. Kroupp, E. Stambulchik, A. Starobinets, I. Uschmann, and Y. Maron, "Determination of the ion temperature in a high-energy-density plasma using the stark effect," *Phys. Rev. Lett.* **122**, 095001 (2019).
- ²⁴G. B. Rybicki and A. P. Lightman, *Radiative Processes in Astrophysics* (Wiley, 1979).